Journal of Power Sources 254 (2014) 98–105

Contents lists available at ScienceDirect

Journal of Power Sources

journal homepage: www.elsevier.com/locate/jpowsour

Efficient quasi-solid-state dye-sensitized solar cells employing polyaniline and polypyrrole incorporated microporous conducting gel electrolytes

Shuangshuang Yuan [a], Qunwei Tang [a,*], Benlin He [a], Peizhi Yang [b]

[a] Institute of Materials Science and Engineering, Ocean University of China, Qingdao 266100, Shandong Province, PR China
[b] Key Laboratory of Advanced Technique & Preparation for Renewable Energy Materials, Ministry of Education, Yunnan Normal University, Kunming 650092, PR China

HIGHLIGHTS

- PANi or PPy is incorporated into 3D framework of microporous PAA–PEG matrix.
- The electrocatalytic reaction of triiodides is conducted into conducting gel electrolyte.
- Liquid electrolyte is driven by osmotic pressure and capillary diffusion.
- An power conversion efficiency of 7.12% is recorded.

ARTICLE INFO

Article history:
Received 27 November 2013
Accepted 24 December 2013
Available online 4 January 2014

Keywords:
Quasi-solid-state dye-sensitized solar cell
Conducting gel electrolyte
Microporous structure
Polyaniline
Polypyrrole

ABSTRACT

With an aim of elevating liquid electrolyte loading, ionic conductivity, and electrocatalytic activity of gel electrolyte toward triiodides, freeze-dried microporous poly(acrylic acid)–poly(ethylene glycol) (PAA–PEG) matrix is employed to uptake conducting polymers, such as polyaniline (PANi) and polypyrrole (PPy). An ionic conductivity of 19.18 mS cm^{-1} at 65 °C is obtained from PAA–PEG/PANi conducting gel electrolyte which is nearly similar to 19.22 mS cm^{-1} from pure liquid electrolyte. The conducting polymers can form interconnected channels within insulating microporous PAA–PEG matrix, therefore, the reduction reaction of triiodide ions in the dye-sensitized solar cells (DSSCs) can be extended from Pt/gel electrolyte interface to both interface and three-dimensional framework of microporous conducting gel electrolyte. The resultant DSSCs from PAA–PEG/PANi and PAA–PEG/PPy conducting gel electrolytes display power conversion efficiencies of 7.12% and 6.53%, respectively, which are much higher than 5.02% from pure PAA–PEG-based DSSC. The new concept along with easy fabrication promises the microporous conducting gel electrolytes to be good alternatives in efficient quasi-solid-state DSSCs.

1. Introduction

As a promising solution to energy depletion, environmental pollution, and ecological destruction, dye-sensitized solar cells (DSSCs) have attracted growing interests because of their merits on easy fabrication, low cost, and relatively high power conversion efficiency [1–3]. A typical DSSC, composing of dye-sensitized TiO_2 anode, Pt counter electrode, and I^-/I_3^- redox species, is an electrochemical device converting solar energy to electricity with no pollutant emission [4]. The leakage of liquid electrolyte and evaporation of organic solvent such as nitriles are always burdens for commercial application of DSSCs [5,6]. By addressing these two issues, full-solid-state electrolytes are preferred candidates in highly stable DSSC devices [7,8]. However, the full-solid-state electrolytes cannot provide a relatively high carrier transport in inorganic electrolytes (hole diffusion) or polymer electrolytes (movement of chain segments), resulting in a decreased redox kinetics. Polymer gel electrolytes, especially the ones formed by imbibing liquid electrolyte into three-dimensional (3D) frameworks of amphiphilic gel matrices combine the rapid ionic transfer of liquid electrolytes and relatively high stability of full-solid-state electrolytes [9–13]. The imbibed liquid electrolyte can migrate within the interconnected microporous structure of gel matrix and cannot leak from the sealed framework during cell fabrication. However, there is still a remaining problem for these gel electrolyte-based DSSCs in Pt counter electrode/gel electrolyte

* Corresponding author. Tel./fax: +86 532 66781690.
E-mail address: tangqunwei@hotmail.com (Q. Tang).

0378-7753/$ – see front matter © 2014 Elsevier B.V. All rights reserved.
http://dx.doi.org/10.1016/j.jpowsour.2013.12.112

interface. In comparison with Pt counter electrode/liquid electrolyte interface, the Pt counter electrode/gel electrolyte interface has an elevated resistance for the electrocatalytic reaction of triiodide ions with refluxed electrons because of the poor contact of polymer gel electrolyte and solid-state Pt counter electrode. In our previous research, we open a concept of extending the electrocatalytic reaction of triiodides from gel electrolyte/Pt counter electrode interface to both interface and 3D framework of conducting gel electrolyte, in which monomers of conducting polymers (such as aniline, pyrrole) are imbibed and in-situ polymerized in the matrices [14–18]. The power conversion efficiency has been significantly enhanced from ~5.5% to ~6.5%. These conducting gel electrolytes suffer from low liquid electrolyte loading and therefore ionic conductivity because the swelling of gel matrices in liquid electrolyte obeys Flory theory [19], in which the driving force of liquid electrolyte is osmotic pressure present across the gel matrices.

Here we report another new concept of employing microporous structure into poly(acrylic acid)–poly(ethylene glycol) (PAA–PEG) semi-interpenetrating (semi-IPN) gel matrix as a way to increase liquid electrolyte loading and therefore ionic conductivity and electrocatalytic activity. To the best of our knowledge, there are no reports on the employment of microporous conducting gel matrices in efficient DSSCs. The loading of liquid electrolyte by PAA–PEG is primarily driven by both osmotic pressure present across the gel matrix and capillary diffusion from micropores [20], resulting an enhanced liquid electrolyte loading. Elevated redox couple loading along with enhanced electrocatalytic activity is expected to provide increased photovoltaic performances of quasi-solid-state DSSCs.

2. Experimental

2.1. Synthesis of PAA–PEG matrices

The PAA–PEG matrices were synthesized according to an aqueous solution polymerization route. In detail, a solution mixture consisting of acrylic acid monomer (8 ml, AA, analytical reagent) and PEG (4.4 g, M_W = 20,000, analytical reagent) was made by agitating in deionized water (15 ml) in a water-bath at 80 °C. Under vigorous agitation, crosslinker *N*,*N*′-(methylene)bisacrylamide (NMBA, 0.008 g) and initiator ammonium persulfate (APS, 0.225 g) were subsequently added to the above mixture. With the proceeding of polymerization, the viscosity increased gradually. When the viscosity of the PAA–PEG reached around 180 mPa s^{-1}, the reagent was poured into a Petri dish and cooled to room temperature with the formation of an elastic transparent gel. The PAA–PEG membranes were then molded into φ 2.5 cm die. After rinsing with deionized water, the membranes were dried under vacuum at 50 °C for 24 h.

2.2. Preparation of PANi and PPy

0.592 ml of aniline was dissolved in 20 ml of 1 M HCl aqueous solution to obtain a homogeneous mixture. 20 ml of 0.125 M APS aqueous solution was dipped in the above mixture within 30 min. The polymerization reaction was carried out at 0 °C. After 3 h, the resultant reactant was rinsed by 1 M HCl aqueous solution, filtrated, and finally vacuum dried at 60 °C for 24 h.

1 ml of pyrrole monomer was dipped in an aqueous solution of $FeCl_3$ containing 7.788 g of $FeCl_3 \cdot 6H_2O$ and 58 ml of deionized water. Under vigorous agitation, the polymerization reaction was carried out at 5 °C for 24 h. After being rinsed by aqueous solution, filtrated, and finally vacuum dried at 60 °C for 24 h, the resultant PPy powders were obtained.

2.3. Preparation of conducting gel electrolytes

The microporous PAA–PEG matrices were prepared by immersing dried PAA–PEG matrices in deionized water for 72 h to reach their swelling equilibrium, and subsequently freeze-dried under vacuum at −60 °C for 72 h. After that the matrices were immersed in liquid electrolyte consisting of redox electrolyte and PANi or PPy for 5 days to reach absorption equilibrium. The contents of PANi and PPy in liquid electrolyte were 2.10 and 1.38 g L^{-1}, respectively. A redox electrolyte consisted of 100 mM of tetraethylammonium iodide, 100 mM of tetramethylammonium iodide, 100 mM of tetrabutylammonium iodide, 100 mM of NaI, 100 mM of KI, 100 mM of LiI, 50 mM of I_2, and 500 mM of 4-*tert*-butyl-pyridine in 50 ml acetonitrile.

2.4. Assembly of quasi-solid-state DSSCs

A layer of TiO_2 nanocrystal anode film with a thickness of 10 μm and active area of 0.09 cm^2 was prepared by coating the TiO_2 colloid using a screen printing technique, followed by sintering in air at 450 °C for 30 min. Subsequently, the TiO_2 film was soaked in a 0.5 mM N719 [cis-di(thiocyanato)-*N*,*N*′-bis(2,2′-bipyridyl-4-carboxylic acid-4-tetrabutylammonium carboxylate], purchased from Dyesol LTD, Australia] ethanol solution for 24 h to uptake N719 dye for the fabrication of dye-sensitized TiO_2 photoanode. The quasi-solid-state DSSCs from PAA–PEG/PANi, PAA–PEG/PPy, or PAA–PEG gel electrolyte at an imbibition equilibrium were fabricated by sandwiching a slice of gel electrolyte with a thickness of around 1 mm between dye-sensitized TiO_2 anode and a Pt counter electrode.

2.5. Photovoltaic measurements

The photocurrent–voltage (*J*–*V*) curves of the assembled quasi-solid-state DSSC were recorded on an electrochemical workstation (CHI600E) under irradiation of a simulated solar light from a 100 W xenon arc lamp in ambient atmosphere. The incident light intensity was calibrated using a FZ-A type radiometer from Beijing Normal University Photoelectric Instrument Factory to control it at 100 mW cm^{-2} (AM 1.5). Each DSSC device was measured five times to eliminate experimental error and a compromise *J*–*V* curve was employed.

2.6. Characterizations

The morphologies of the gel electrolytes were captured with a Zeiss Ultra plus field emission scanning electron microscopy (FESEM). To observe the internal 3D microstructure, swollen gel electrolytes were first cut into ultrathin film, followed by the loading into a chamber under freezing temperature and high vacuum to remove solvent. Fourier transform infrared spectrometry (FTIR) spectra were recorded on a Vertex 70 FTIR spectrometer (Bruker). The ionic conductivity of gel electrolyte was measured by using a pocket conductivity meter (DSSJ-308A, LeiCi Instruments). The instrument was calibrated with 0.01 M KCl aqueous solution prior to experiments. Tafel polarization curves of the symmetrical cells fabricated of samples were measured by CHI660E electrochemical workstation. The symmetrical dummy cells fabricated with two identical Pt electrodes (Pt electrode/gel electrolyte/Pt electrode). The electrochemical impedance spectroscopy (EIS) was carried out using a CHI660E electrochemical workstation at a constant temperature of 20 °C with an ac signal amplitude of 20 mV in the frequency range from 0.1 to 10^5 Hz at 0 V dc bias in the dark. The cyclic voltammetry (CV) was also carried out on a CHI660E electrochemical workstation in a N_2-purged liquid electrolyte. The

CV curves were scanned by two methods: (i) owing to an incorporation of PANi or PPy, the conducting gel electrolyte was used as a working electrode because it was an electron-conducting material; (ii) a Pt wire was pierced into the conducting gel electrolyte and employed as a working electrode. The depth of Pt wire in gel electrolyte was controlled at 1 cm. In the two approaches, Pt foil and an Ag/AgCl electrode were used as counter electrode and reference electrode, respectively. The supporting electrolyte was 0.1 M $LiClO_4$ whereas the redox couple was 10 mM LiI and 1 mM I_2. All the curves were scanned at a scan rate of 50 mV s^{-1}. Incident photo-to-current conversion efficiency (IPCE) curves were obtained at the short-circuit condition on an IPCE measurement systems (MS260). The light source in this case was a solar simulator (PEC-L11, AM1.5G, Peccell Technologies, Inc.); Light was focused through a monochromator onto the photovoltaic cell. The monochromator was moved in steps from 400 to 700 nm to generate the IPCE. In order to obtain the IPCE spectra, the anodes were sensitized by N719 dye.

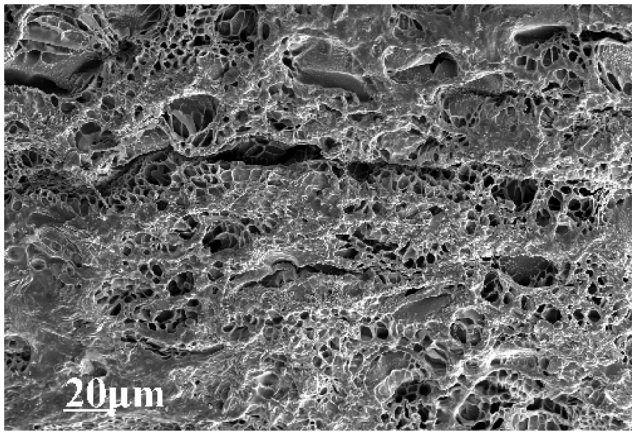

Fig. 2. SEM photograph of microporous PAA–PEG semi-IPN matrix.

3. Results and discussion

3.1. Structural analysis

The synthesis of PAA–PEG matrix is a simple process schematically illustrated in Fig. 1. Owing to the macrobiradical nature of NMBA, AA monomers can be polymerized into a 3D PAA framework, whereas PEG is still a linear structure. Therefore, resulting PAA–PEG matrix is a semi-IPN structure accompanied by H-bonding interactions between C=O (PAA) and–OH (PEG), and between –OH (PAA) and –O– (PEG), suggesting that the partial loss of hydrophilicity and appearance of amphiphilicity.

The cross-sectional SEM image of PAA–PEG semi-IPN matrix is shown in Fig. 2, suggesting that the PAA–PEG matrix has an interconnected and microporous structure capable of caging enormous liquid electrolyte in the micropores. The imbibition of liquid electrolyte by PAA–PEG semi-IPN is primarily driven by the osmotic pressure across the gel matrix and capillary diffusion from micropores [20]. The microporous PAA–PEG surface conserve hydrophilicity and hydrophobicity and allows the use of capillary forces for filling the liquid electrolyte into the micropores. However, the diffused liquid electrolyte will be further imbibed by the amphiphilic PAA–PEG framework, resulting in the stretch and relaxation of PAA–PEG matrix chains in liquid electrolyte with expansion in volume. Owing to the nature of interconnected framework, PANi or PPy molecular chains can also diffuse into PAA–PEG matrix, forming conducting gel electrolytes.

The FTIR spectra of PAA–PEG/PANi, PAA–PEG/PPy, and PAA–PEG matrix are shown in Fig. 3, where the absorption bands at 1663, 1510, 1467, and 1115 cm^{-1} in pure PAA–PEG matrix are originated from the vibrations of C=O stretching (PAA), C=O bending (PAA), O–H distorting (PAA), and C–O–C stretching (PEG),

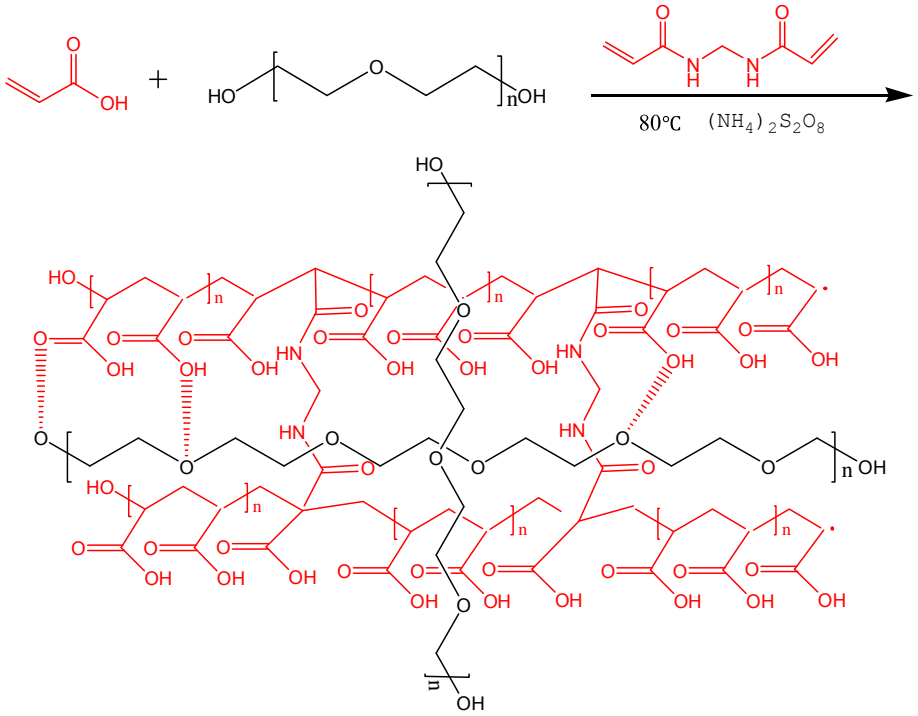

Fig. 1. Schematic of polymerization of PAA–PEG matrix.

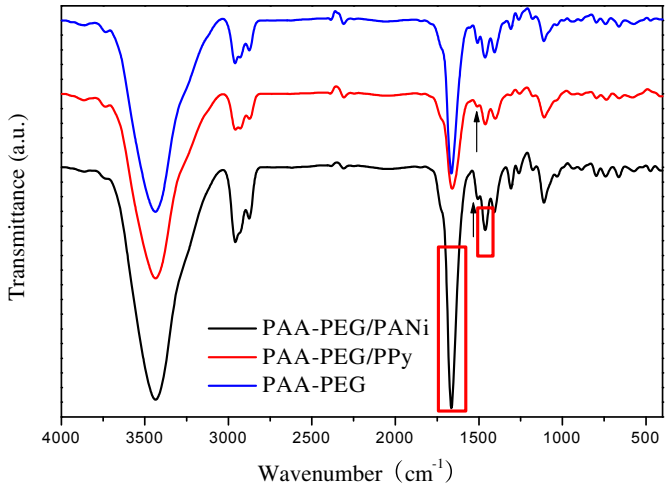

Fig. 3. FTIR spectra of PAA–PEG/PANi, PAA–PEG/PPy, and PAA–PEG matrix.

respectively [21]. However, the bands intensities of 1663 cm^{-1} are elevated because of the overlap of C=C stretching deformation mode of quinoid in PAA–PEG/PANi and C=C stretching vibration in PAA–PEG/PPy, indicating that the PANi and PPy have been diffused into gel matrices [22]. However, the band intensities attributing to C=O bending of PAA are decreased, which is a signal that the H-bonding between PAA and PEG restricts the vibration of C=O bonds.

3.2. Liquid electrolyte loading

The imbibition kinetics of microporous PAA–PEG in various liquid electrolytes, shown in Fig. 4, is mainly due to the Flory theory from osmotic pressure across the matrix and capillary diffusion from micropores. The liquid electrolyte loading increases with elongation of imbibition time, indicating a gradual diffusion of liquid electrolyte into PAA–PEG semi-IPN matrix. An absorption equilibrium can be obtained at swelling time of around 30 h, and no further diffusion occurs under longer immersion time. In order to determine the nature of liquid electrolyte loading by PAA–PEG, the accumulative H_3PO_4 loading over time have been fitted using the Fickian theory [23].

$$\frac{M_t}{M_\infty} = kt^n$$

where M_t and M_∞ are the mass of the imbibed liquid electrolyte at time t and at equilibrium, respectively. K is a characteristic rate constant relating to the properties of PAA–PEG matrix, and n is a transport number characterizing the transport mechanism. $n \leq 0.5$ suggests a Fickian or Case I transport behavior in which the PAA–PAA relaxation is much faster than the diffusion; $n = 1$ gives a non-Fickian or Case II mode of transport where liquid electrolyte uptake is controlled by diffusion process. $0.5 < n < 1$ refers to an anomalous or a Case III mode in which structural relaxation is comparable to diffusion. By plotting $\log(M_t/M_\infty)$ vs $\log(t)$, the n values are recorded and shown in inserts. The n values from the PAA–PEG semi-IPN matrix by swelling in various liquid electrolytes are

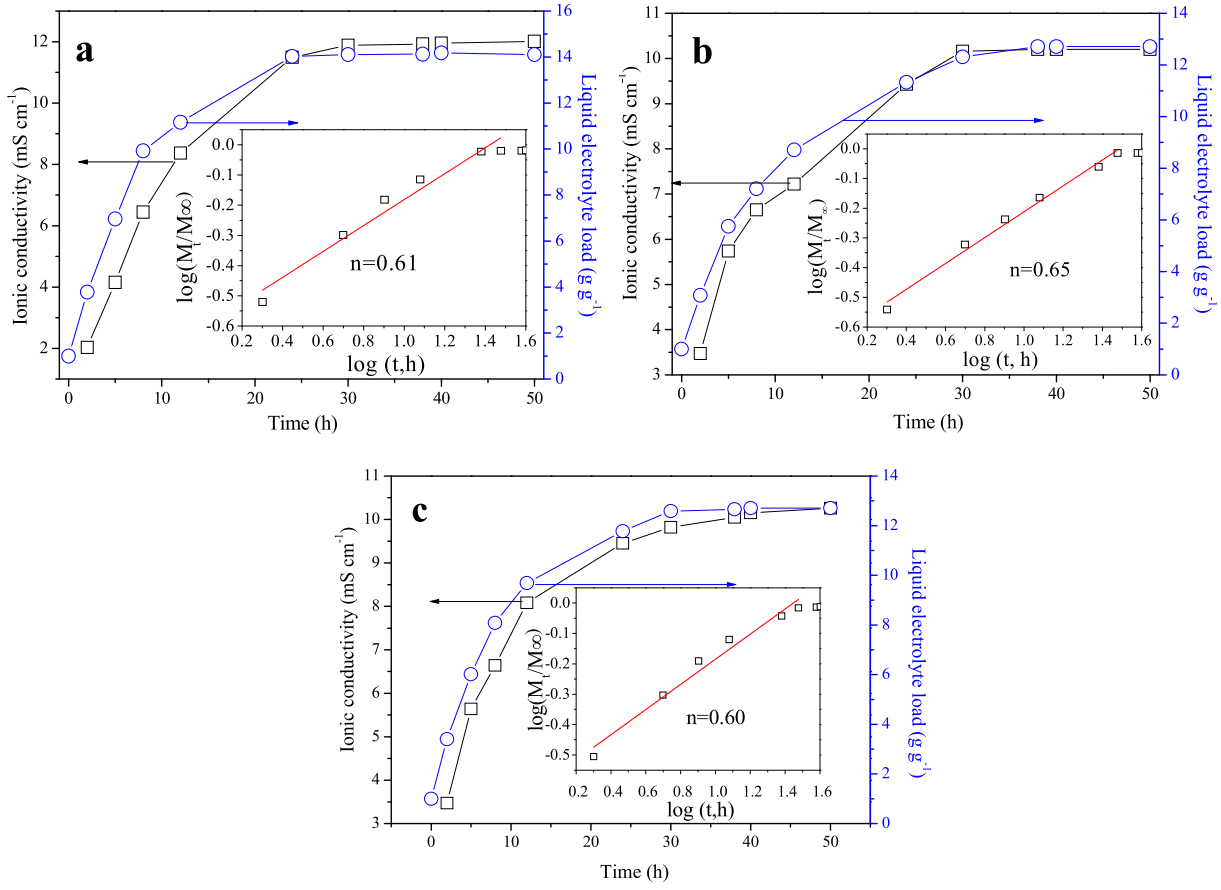

Fig. 4. Imbibition kinetics of PAA–PEG matrix to various liquid electrolytes: (a) PAA–PEG in PANi-containing liquid electrolyte, (b) PAA–PEG in PPy-containing liquid electrolyte, and (c) PAA–PEG in pure liquid electrolyte. The insert shows the imbibition kinetics of various gel electrolytes.

higher than 0.5, indicating an anomalous mechanism mode in which structural relaxation is comparable to diffusion. The result indicates that the loading of liquid electrolyte is controlled by osmotic pressure. From the loading of liquid electrolyte, it is apparent that the PAA–PEG/PANi has a loading of 14.11 g g^{-1}, which is much higher than 12.71 and 12.70 g g^{-1} for PAA–PEG/PPy, and PAA–PEG. Higher liquid electrolyte loading indicates a higher content of liquid electrolyte in per unit of volume and enhanced ionic conductivity. A room-temperature ionic conductivity is 12.01 mS cm^{-1} for PAA–PEG/PANi gel electrolyte, which is also the highest in the three gel electrolytes.

3.3. Ionic conductivity

The ionic conductivity and activation energy, E_a, are key parameters in elevating the performances of a gel electrolyte [24]. The proton conductivity–temperature plots of various gel electrolytes as well as pure liquid electrolyte follow an Arrhenius relationship reasonably well as shown in Fig. 5 [25]. E_a values in the three gel electrolytes systematically decrease with imbibition time of liquid electrolyte. Low E_a value in gel electrolyte suggests a facile ionic transport along conducting channels. It is reasonable that the conducting channels tend to be interconnecting at higher imbibition aging because of gradual diffusion and attachment of PANi or PPy within PAA–PEG semi-IPN matrix. Therefore, the interconnected pore structure of PAA–PEG semi-IPN provides superhighway for efficient ion transport. Moreover, the E_a values from PAA–PEG/PANi and PAA–PEG/PPy are much lower and closer than that from PAA–PEG gel electrolyte and pure liquid electrolyte. According to Fig. 5, the ionic conductivities at 65 °C are 19.18 mS cm^{-1} (PAA–PEG/PANi), 18.41 mS cm^{-1} (PAA–PEG/PPy), and 17.30 mS cm^{-1} (PAA–PEG), whereas that is 19.22 mS cm^{-1} for pure liquid electrolyte. The decreased E_a and increased ionic conductivity are expected to significantly enhance the reaction kinetics of DSSCs.

3.4. Electrochemical characterizations

With an aim of validating the electrocatalytic behaviors of PAA–PEG/PANi and PAA–PEG/PPy conducting gel electrolytes, CV curves were recorded by two approaches: (i) conducting gel electrolyte was used as a working electrolyte which was immersed in the liquid electrolyte. The recorded redox peaks should be attributed to the electrocatalytic activity of conducting gel electrolyte toward triiodides; (ii) a Pt wire was pierced into conducting gel electrolyte by controlling the depth of 1 cm. Such Pt pierced conducting gel electrolyte was employed as a working electrode by connecting the Pt on electrochemical workstation. In this state, the scanned redox peaks were from the comprehensive electrocatalytic activity of Pt wire and conducting gel electrolyte toward triiodides. However, the function of Pt wire toward redox species was the same because of the same depth in gel electrolyte, therefore, we could also assess the electrocatalytic behaviors of conducting gel electrolyte. Moreover, we could determine whether the imbibed ionic liquid was "flowable" or "exchangeable" within the 3D framework of conducting gel electrolyte. As a reference, the CV curves from PAA–PEG gel electrolyte were also determined at the same conditions. As shown in Fig. 6a, no redox peaks are observed from PAA–PEG gel

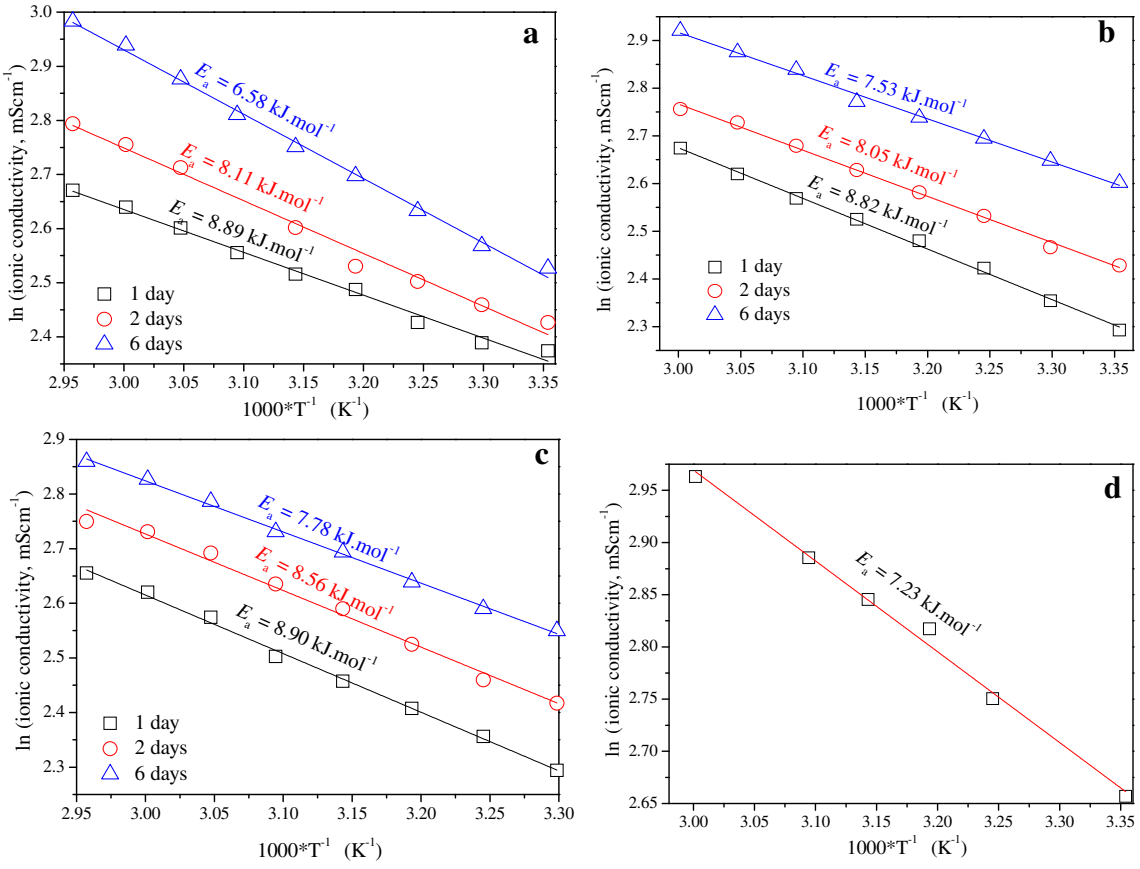

Fig. 5. Arrhenius plots of various gel electrolytes: (a) PAA–PEG/PANi, (b) PAA–PEG/PPy, (c) PAA–PEG, and (d) pure liquid electrolyte.

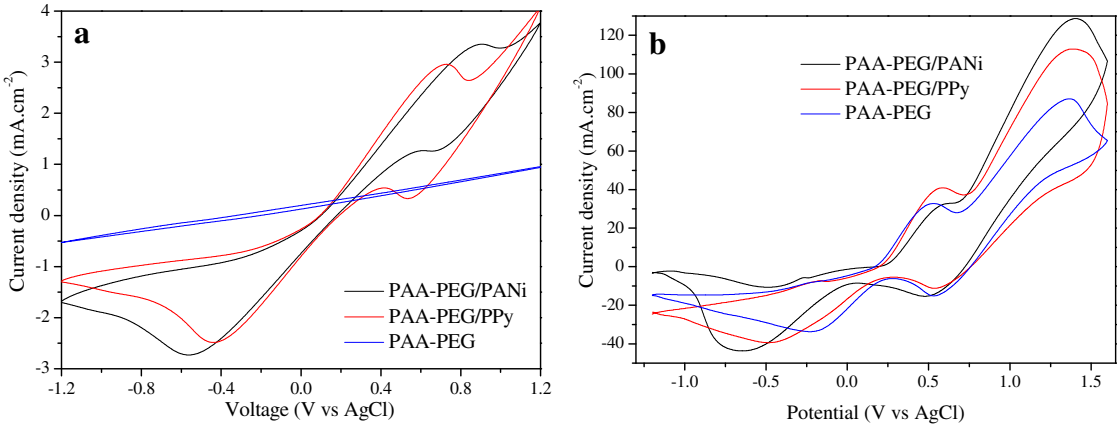

Fig. 6. (a) CV curves for gel electrolytes recorded from various gel electrolytes. (b) CV curves of gel electrolytes using a pierced Pt wire as working electrode. All the curves were scanned at a scan rate of 50 mV s^{-1}.

electrolyte because of its non-electrically conducting performance. Interestingly, a couple of redox peaks are recorded in either PAA–PEG/PANi or PAA–PEG/PPy conducting gel electrolyte, indicating that the conducting gel electrolytes have electrocatalytic activities toward triiodides. The electrocatalytic performances of conducting gel electrolyte result from the incorporation of PANi or PPy in 3D framework of PAA–PEG semi-IPN [26,27]. A new approach of confirming the migration of I^-/I_3^- redox couples within interconnected 3D PAA–PEG semi-IPN is shown in Fig. 6b, in which CV curves are recorded using a pierced Pt wire as working electrode. Two couples of redox peaks are determined in each gel electrolyte, indirectly reflecting that the I^-/I_3^- redox couples can migrate in the interconnected 3D framework of PAA–PEG matrix. The rapid migration of redox species within 3D framework of PAA–PEG/PANi or PAA–PEG/PPy can accelerate their redox reaction kinetics and therefore elevate the photovoltaic performances of DSSC devices. Moreover, the peak current density from PAA–PEG/PANi is the highest among three gel electrolytes. This may be the synergistic effect of PANi and Pt on electroreduction reaction of I^-/I_3^- redox couples.

The charge-transfer ability of the conducting gel electrolytes can be confirmed by EIS measurement, as shown in Fig. 7a, an asymmetric sandwich cell composed of a gel electrolyte sandwiched by two FTO supported Pt glass electrodes. The charge transfer resistances (R_{ct}, the first semicircle) of conducting gel electrolytes are much lower than that of PAA–PEG. Lower R_{ct} reveals that the charge-transfer ability in conducting gel electrolyte/Pt interface is higher than that in PAA–PEG/Pt interface [28]. The rapid transport of refluxed electrons from Pt counter electrode to gel electrolyte is expected to accelerate the reduction reaction of iodides.

Tafel polarization plots were also recorded to determine the electrocatalytic activity of the gel electrolytes, which was also performed with the asymmetric similar to those used in EIS measurements, are shown in Fig. 7b. A larger slope in the anodic or cathodic branch indicates a higher exchange current density (J_0) and better electrocatalytic activity toward redox couples on the gel electrolytes. It is obvious that the J_0 value is in an order of PAA–PEG/PANi > PAA–PEG/PPy > PAA–PEG, which is consistent with R_{ct} in EIS spectra.

3.5. Photovoltaic performances

The *J–V* characteristics of the quasi-solid-state DSSCs from PAA–PEG/PANi, PAA–PEG/PPy, and PAA–PEG gel electrolytes are presented in Fig. 8 and the corresponding photovoltaic parameters are summarized in Table 1. The power conversion efficiencies of DSSCs from PAA–PEG/PANi and PAA–PEG/PPy are 7.12% and 6.53%, respectively, which are much higher than 5.02% from PAA–PEG and other non-conducting gel electrolyte based DSSCs [29–31]. As mentioned above, the incorporation of electrically conducting PANi and PPy with insulating microporous PAA–PEG matrix can elevate liquid loading, enhance charge-transfer ability and electrochemical

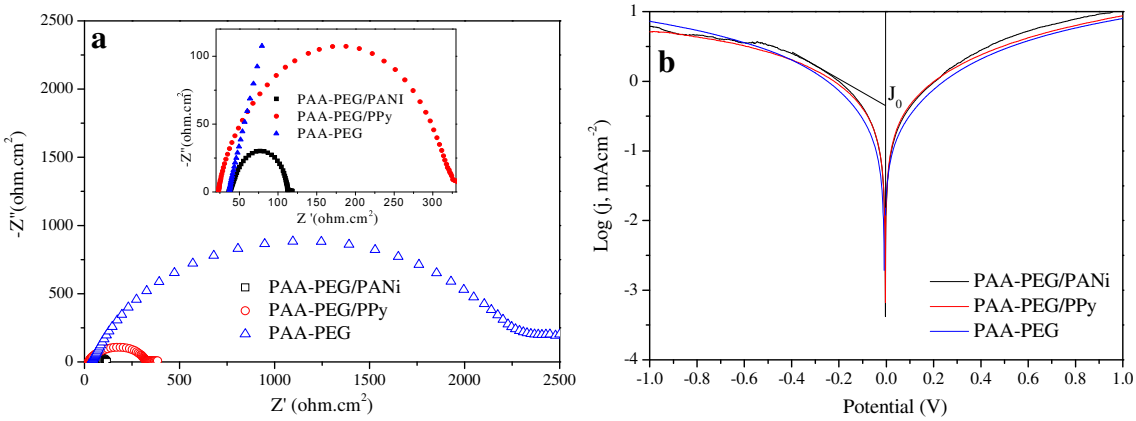

Fig. 7. (a) Nyquist plots and (b) Tafel polarization curves of PAA–PEG/PANi, PAA–PEG/PPy, and PAA–PEG gel electrolytes.

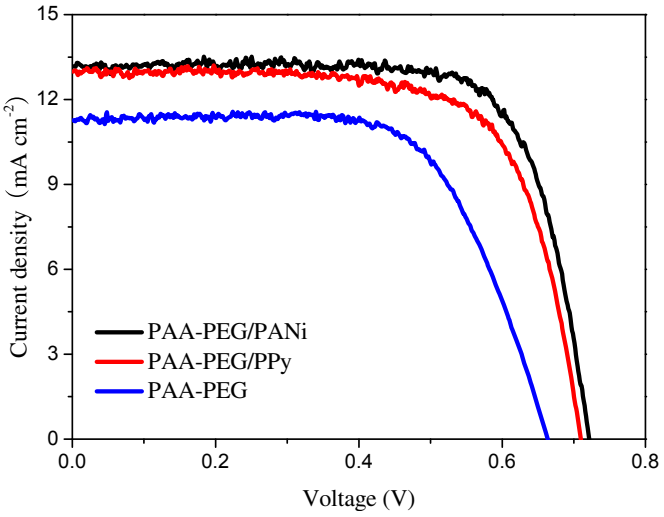

Fig. 8. Photocurrent–voltage characteristics curves of quasi-solid-state DSSCs from PAA–PEG/PANi, PAA–PEG/PPy, and PAA–PEG gel electrolytes.

Table 1
The photovoltaic performances of the quasi-solid-state DSSCs based on different gel electrolytes.

Gel electrolytes	V_{oc} (mV)	J_{sc} (mA cm^{-2})	*FF*	η
PAA–PEG/PANi	722	13.25	0.74	7.12
PAA–PEG/PPy	710	12.96	0.71	6.53
PAA–PEG	663	11.25	0.67	5.02

activity toward triiodides. Therefore, the quasi-solid-state DSSCs from conducting gel electrolyte have predominant photovoltaic performances. Moreover, V_{oc} is determined by the energy level difference between the Fermi level of the electron in the photoanode and the redox potential of the electrolyte, whereas the real V_{oc} of the DSSCs is smaller than this theoretical limit, and a main reason is a backward reaction between dye molecules and electrolyte. The deviation of V_{oc} may be attributed to the difference of three gel electrolytes in suppressing electron–ion recombination.

In order to evaluate the origin of variation in photocurrent from conducting gel electrolytes, the IPCE spectra of monolithic DSSCs were recorded. As is shown in Fig. 9, the IPCE value is increased in PAA–PEG/PANi and PAA–PEG/PPy gel electrolytes which is mainly due to the enhanced ionic conductivity and triiodide diffusion coefficient [32,33]. From the IPCE curves, one can see that the PAA–PEG/PANi gel electrolyte has the highest ionic conductivity and microporous structure for triiodide diffusion, which is in a good agreement with electrical tests and CV analysis.

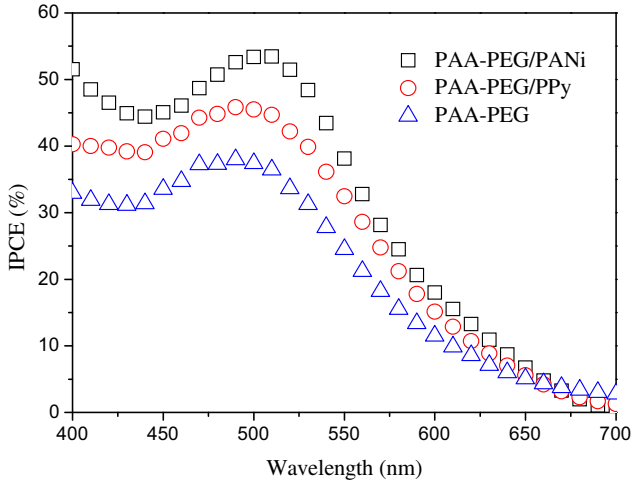

Fig. 9. IPCE curves of the DSSCs from PAA–PEG/PANi, PAA–PEG/PPy, and PAA–PEG gel electrolytes.

4. Conclusions

Conducting gel electrolytes from PAA–PEG/PANi and PAA–PEG/PPy have been fabricated using the microporous structure and imbibition capacity of amphiphilic PAA–PEG matrix to liquid electrolyte. The electrical and electrochemical characterizations indicated that the ionic conductivity and electrocatalytic activity toward iodides have been both significantly enhanced. The electrocatalytic reaction of iodides was also extended from gel electrolyte/Pt interface to both interface and 3D framework of conducting gel electrolyte. The highest power conversion efficiency of 7.12% was obtained from the DSSC using PAA–PEG/PANi gel electrolyte in comparison with 6.53% from PAA–PEG/PPy and 5.02% from pure PAA–PEG based DSSCs. This research opens a gateway to improve the photovoltaic performances of DSSCs and highlights competitive capacity of the quasi-solid-state DSSCs among photovoltaic devices.

Acknowledgments

The authors gratefully acknowledge Ocean University of China for providing Seed Fund to this project, and Fundamental Research Funds for the Central Universities (201313001, 201312005), Shandong Province Outstanding Youth Scientist Foundation Plan (BS2013CL015), Doctoral Fund of Ministry of Education of China (20130132120023), Shandong Provincial Natural Science Foundation (ZR2011BQ017), Research Project for the Application Foundation in Qingdao (13-1-4-198-jch), and Natural Science Foundation of China (U1037604).

References

[1] B. O'Regan, M. Grätzel, Nature 353 (1991) 737–740.
[2] U. Bach, D. Lupo, P. Comte, J.E. Moser, F. Weissortel, J. Salbeck, M. Grätzel, Nature 395 (1998) 583–585.
[3] M. Grätzel, Nature 414 (2001) 338–344.
[4] J.N. Freitas, A.F. Nogueira, M.A.D. Paoli, J. Mater. Chem. 19 (2009) 5279–5294.
[5] H.S. Chen, S.J. Lue, Y.L. Tung, K.W. Cheng, F.Y. Huang, K.C. Ho, J. Power Sources 196 (2011) 4162–4172.
[6] M. Wang, X. Pan, X. Fang, L. Guo, C. Zhang, Y. Huang, Z. Huo, S.Y. Dai, J. Power Sources 196 (2011) 5784–5791.
[7] C. Longo, A.F. Nogueira, M.A.D. Paoli, H. Cachet, J. Phys. Chem. B 106 (2002) 5925–5930.
[8] C.L. Chen, T.W. Chang, S.C. Su, H. Teng, Y.L. Lee, J. Power Sources 247 (2014) 406–411.
[9] J. Shi, S. Peng, J. Pei, Y. Liang, F. Cheng, J. Chen, ACS Appl. Mater. Interfaces 1 (2009) 944–950.
[10] C.L. Chen, T.W. Chang, H. Teng, C.G. Wu, C.Y. Chen, Y.M. Yang, Y.L. Lee, Phys. Chem. Chem. Phys. 15 (2013) 3640–3645.
[11] R.X. Dong, S.Y. Shen, H.W. Chen, C.C. Wang, P.T. Shih, C.T. Liu, R. Vittal, J.J. Lin, K.C. Ho, J. Mater. Chem. A 1 (2013) 8471–8478.
[12] D. Saikia, C.C. Han, Y.W. Chen-Yang, J. Power Sources 185 (2008) 570–576.
[13] Z. Lan, J.H. Wu, J.M. Lin, M.L. Huang, J. Power Sources 164 (2007) 921–925.
[14] Q.H. Li, H. Chen, L. Lin, P. Li, Y. Qin, M. Li, B. He, L. Chu, Q.W. Tang, J. Mater. Chem. A 1 (2013) 5326–5332.
[15] Q.H. Li, X. Chen, Q.W. Tang, H. Xu, B.L. He, Y. Qin, J. Mater. Chem. A 1 (2013) 8055–8060.
[16] Q.H. Li, X. Chen, Q.W. Tang, H.Y. Cai, Y. Qin, B.L. He, M. Li, S. Jin, Z. Liu, J. Power Sources 248 (2014) 923–930.
[17] Q.H. Li, Q.W. Tang, L. Lin, X. Chen, H. Chen, L. Chu, H. Xu, M. Li, Y. Qin, B.L. He, J. Power Sources 245 (2014) 468–474.
[18] Q.H. Li, Q.W. Tang, N. Du, Y. Qin, J. Xiao, B.L. He, H. Chen, L. Chu, J. Power Sources 248 (2014) 816–821.

[19] P.J. Flory, Principles of Polymer Chemistry, Cornel University Press, New York, 1953.
[20] Q.W. Tang, S.S. Yuan, H.Y. Cai, J. Mater. Chem. A 1 (2013) 630–636.
[21] Q.W. Tang, X.M. Sun, Q.H. Li, J.M. Lin, J.H. Wu, J. Mater. Sci. 44 (2009) 726–733.
[22] Q.W. Tang, J.H. Wu, X.M. Sun, Q.H. Li, J.M. Lin, Langmuir 25 (2009) 5253–5257.
[23] N.W. Franson, N.A. Peppas, J. Appl. Polym. Sci. 28 (1983) 1299–1310.
[24] J. Yoon, D. Kang, J. Won, J.Y. Park, Y.S. Kang, J. Power Sources 201 (2012) 395–401.
[25] T.M.W.J. Bandara, M.A.K.L. Dissanayake, I. Albinsson, B.E. Mellander, J. Power Sources 195 (2010) 3730–3734.
[26] Q.W. Tang, H.Y. Cai, S.S. Yuan, X. Wang, J. Mater. Chem. A 1 (2013) 317–323.
[27] J. Xia, L. Chen, S. Yanagida, J. Mater. Chem. 21 (2011) 4644–4649.
[28] H. Anwar, A.E. George, I.G. Hill, Sol. Energy 88 (2013) 129–136.
[29] J.E. Benedetti, A.A. Correa, M. Carmello, L.C.P. Almeida, A.S. Goncalves, A.F. Nogueira, J. Power Sources 208 (2012) 263–270.
[30] Y. Zhang, J. Zhao, B. Sun, X. Chen, Q. Li, L. Qiu, F. Yan, Electrochim. Acta 61 (2012) 185–190.
[31] J.E. Benedetti, A.D. Goncalves, A.L.B. Formiga, M.A.D. Paoli, X. Li, J.R. Durrant, A.F. Nogueira, J. Power Sources 195 (2010) 1246–1255.
[32] X. Huang, Y. Liu, J. Deng, B. Yi, X. Yu, P. Shen, S. Tang, Electrochim. Acta 80 (2012) 219–226.
[33] M.S. Kang, K.S. Ahn, J.W. Lee, J. Power Sources 180 (2008) 896–901.